Numerical investigation on the effect of stroke plane inclination on the aerodynamic performance of dragonfly take-off flight

Shubham Tiwari[1*] *Sejal Madan*[2], and *Sunil Chandel*[1]

[1] Department of Mechanical Engineering, Defence Institute of Advanced Technology (DU), Pune – 411025, India
[2] Department of Information Technology, Guru Nanak Dev Engineering College, Ludhiana, Punjab – 141006, India

Abstract. A numerical investigation is carried out to study the role of inclined stroke plane on the aerodynamic performance of a dragonfly during a take-off flight. A two-dimensional numerical simulation of tandem foils oscillating in-phase along an inclined stroke plane at $Re = 160$ is performed using ANSYS Fluent. The stroke plane angle is varied from $10^o \leq \beta \leq 80^o$ to determine its effect on aerodynamic force coefficients of forefoil and hindfoil. The result shows that the presence of forefoil reduces the hindfoil C_V for low stroke plane angle cases. The cycle-average vertical force coefficient $\overline{C_V}$ of both foils increases with β up to 50° and then decreases. A vortex pair is present in the wake of the foils during each cycle, which induces a downward dipole jet. The dipole jet characteristics such as jet width, location and maximum velocity components are measured for each stroke plane angle. It is observed that the cause of variation in $\overline{C_V}$ and $\overline{C_H}$ with stroke plane angle can be explained with the help of dipole jet characteristics.
Keywords: Dragonfly, forewing, hindwing, take-off, inclined stroke plane

1 Introduction

Flying insects utilize a flapping wing system to generate lift and thrust necessary for a controlled flight. Understanding the underlying principle behind their flight is of fundamental interest for developing Micro Air Vehicles (MAVs). The unsteady aerodynamics associated with insect flight has been studied extensively due to the complex nature of their wing kinematics and their outstanding flying capability.

Dragonflies are unique among the other flying insect as they have remarkable agility and rapid maneuvering abilities. Dragonfly flight has been a focus of research for the past five decades [1-3]. Wang [4] performed a two-dimensional computational study of a dragonfly hovering at Re=157 and studied the effect of wing kinematics by varying the stroke plane angle and mean pitch angle so that the resultant force is vertically upward. It showed that the

* Corresponding author: shubh6tiwari@gmail.com

drag plays a vital role by supporting 75 % of insect weight and a downward dipole jet is generated, which becomes faster and narrower with increasing stroke plane angle.

The three-dimensional shape and kinematics of dragonfly wings result in a highly complex flow structure. Its analysis in 2D can help us understand the significance of 3D flow features at a low Reynolds number. The aerodynamic forces and flow features obtained from the 2D numerical simulation of the flapping wing are consistent with the 3D experimental observations [5]. Deepthi and Vengadesan [6] performed a 2D numerical simulation of an insect wing hovering with different stroke plane angles at $Re = 157$. They studied the characteristics of downward dipole jet generated at different stroke plane angles and its effect on vertical force coefficient. The maximum vertical force coefficient is obtained at the stroke plane angle of 60°, consistent with the experimental observation.

The take-off flight requires a large amount of force to be generated so the insect can become airborne. To achieve this, the insect utilizes different approaches for the take-off, such as flapping with leg jump, clap and fling and slow take-off. Li et al. [7] recorded the voluntary take-off flight of a dragonfly using two high-speed cameras, which showed that the dragonfly has the ability to take off after one wingbeat only. They observed that dragonfly flaps their wings with zero phase difference during take-off and the angle of attack of both wings during the downstroke is significantly larger than the forward flight. The results also showed that the stroke plane angle of forewing and hindwing varied considerably during the take-off procedure. Also, Shanmugam and Sohn [8] found that in-phase stroking with a large angle of attack during downstroke helps generate a higher vertical force coefficient, which is beneficial during take-off flight.

We note from the literature that there have been very limited studies on the dragonfly take-off as well as its stroke plane inclination, an essential mode of flight involving rapid acceleration. Hence, in this study, a two-dimensional numerical simulation is performed for two elliptical airfoils in tandem arrangement oscillating in-phase along an inclined stroke plane at $Re = 160$. The role of stroke plane angle is examined in the aerodynamic performance of dragonflies during take-off flight. Vortex dynamics is studied to understand the role of the downward dipole jet on aerodynamic force generation.

2 Numerical Methodology

2.1 Foil kinematics

An elliptically shaped airfoil is considered with a thickness to chord ratio of 0.1 to represent the cross-section of a dragonfly wing. The foil kinematics used in this study, shown in figure 1, is based on the previous numerical studies and experimental observations [4,7]. The pitch center is located at a half-chord distance from the leading edge of the airfoil. During in-phase oscillation of the foils, the foil spacing of $1.3c$ generates the maximum lift [8,9]. Therefore, the distance between the stroke plane of both airfoils, denoted by L, is $1.3c$.

The flapping kinematics of dragonfly wings is represented by the motion of forefoil and hindfoil undergoing both translational as well as pitching along an inclined stroke plane based on the equations of motion as follows:

For forefoil

$$x_f(t) = \frac{A_o}{2} cos(\beta_f) + \frac{A_o}{2} cos\ (2\pi f t)\, cos(\beta_f) \quad [1]$$

$$y_f(t) = \frac{A_o}{2} sin(\beta_f) + \frac{A_o}{2} cos(2\pi f t)\, sin(\beta_f) \quad [2]$$

$$\alpha_f(t) = \alpha_o + \alpha_m cos\ (2\pi f t + \pi/2) \quad [3]$$

For hindfoil

$$x_h(t) = \frac{A_o}{2} cos(\beta_h) + \frac{A_o}{2} cos\ (2\pi ft + \psi)\ cos(\beta_h) \quad [4]$$

$$y_h(t) = \frac{A_o}{2} sin(\beta_h) + \frac{A_o}{2} cos(2\pi ft + \psi)\ sin(\beta_h) \quad [5]$$

$$\alpha_h(t) = \alpha_o + \alpha_m cos\ (2\pi ft + \pi/2 + \psi) \quad [6]$$

Here, $x(t)$ and $y(t)$ represent the instantaneous displacement of the airfoils along x- and y-axis, respectively, whereas $\alpha(t)$ represents the instantaneous pitch angle relative to stroke plane. The stroke plane angle β is the angle between the stroke plane and the direction of freestream velocity U_∞. A_o represents the flapping amplitude along the stroke plane. The flapping frequency is represented by f and the phase difference between the flapping foils is represented by ψ, which is zero for in-phase oscillation during take-off. α_o is the initial pitch angle and α_m represents the pitch amplitude.

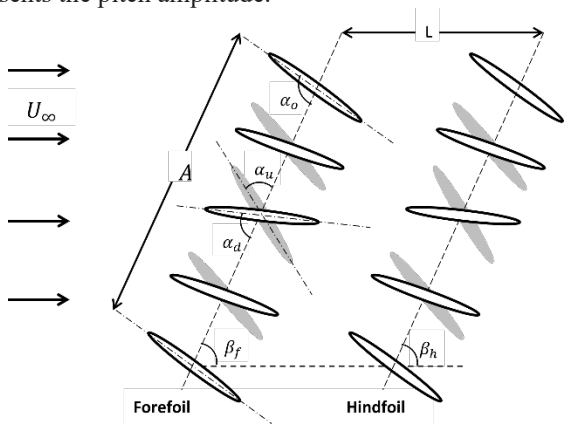

Figure 1: The schematic diagram for forefoil and hindfoil kinematics. White ellipses represent downstroke motion, while grey ellipses denote upstroke motion.

2.2 Computational model

In the present numerical simulation, the flow is considered two-dimensional unsteady and incompressible. The one-equation Spalart-Allmaras (S-A) model is employed to study the flow field evolution. The flow is governed by the continuity equation (eq. 7) and the Navier-Stokes equation (eq. 8).

$$\nabla \cdot u = 0 \quad [7]$$

$$\frac{\partial u}{\partial t} + (u \cdot \nabla)u + \nabla p - \frac{1}{Re}\nabla^2 u = 0 \quad [8]$$

Where u and p represent fluid velocity and pressure, respectively. Equations [7] and [8] are solved using a pressure-based solver in ANSYS Fluent 17.2 software. Pressure-velocity coupling is achieved by using a second-order PISO scheme. The spatial discretization of pressure and momentum is performed using a second-order upwind scheme. The first-order implicit scheme is used for temporal discretization.

The simulation is carried out in a square-shaped computational domain of size $60c \times 60c$, as shown in figure 2. The computational domain is divided into two circular moving zones and an external stationary zone with a non-conformal sliding interface between the moving and stationary zones to allow relative motion. Using this technique, mesh deformation takes place only in the stationary zone. No-slip condition is applied on the surface of both foils. The inlet and outlet are set as velocity inlet and pressure outlet, respectively, whereas the side boundaries are set as symmetry. The motion of both foils and their respective circular zone, as defined by equations [1-6], is achieved by implementing

User-Defined Functions (UDFs) at each time step. The mesh inside the stationary zone is updated using a diffusion-based smoothing method and the remeshing is performed when the skewness of any cell exceeds a user-input value.

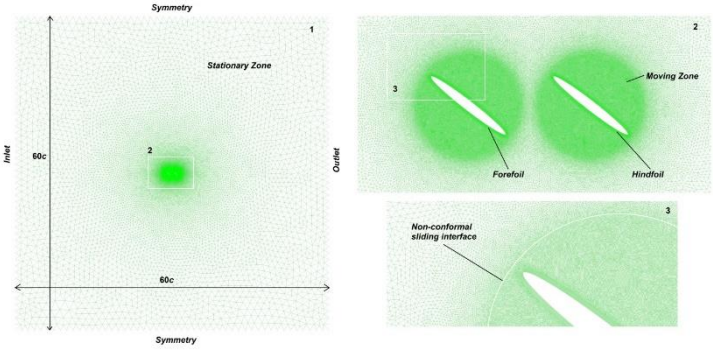

Figure 2: Computational domain with different mesh zones and boundary conditions for present numerical simulation

The Reynolds number is 160 based on freestream velocity and chord length c $(= 0.01\ m)$. The maximum translational velocity of the foil is represented by $U_F = \pi A_o f$. The advanced ratio (J) is the ratio of freestream velocity and maximum translational velocity. The reference velocity is given by U_R $(= U_\infty + U_F)$.

The pressure coefficient (C_P) and the aerodynamic force coefficients are calculated using the following equations:

$$C_P = \frac{P - P_\infty}{0.5\rho {U_R}^2} \quad [9]$$

$$C_V = \frac{F_V}{0.5\rho {U_R}^2 c} \quad [10]$$

$$C_H = \frac{F_H}{0.5\rho {U_R}^2 c} \quad [11]$$

Where C_V and C_H are the instantaneous vertical and horizontal force coefficient, respectively. F_V and F_H are the instantaneous vertical and horizontal forces, respectively and ρ is the fluid density. The cycle-average vertical and horizontal force coefficients are represented by $\overline{C_V}$ and $\overline{C_H}$, respectively.

2.3 Grid Independence study & Validation

A grid independence study is performed to ensure that numerical simulation results are independent of the number of mesh elements and time step size. We tested three cases with a different number of mesh elements as well as time step size for a case of in-phase stroke of forefoil and hindfoil with the parameters: $A_o/c = 2.5$, $\beta = 80^o$, $L = 1.3c$, $\alpha_0 = 105^o$, $\alpha_m = 19^o$ (during downstroke), $\alpha_m = 25^o$ (during upstroke), $f = 30\ Hz$, $J = 0.1$ and $Re = 160$. As given in table 1, the maximum difference in the value of $\overline{C_V}$ (total) for cases 2 and 3 is nearly 0.5%. Therefore, the mesh and time step of case 2 is selected for further simulations.

Table 1: Grid and Time-Step Convergence Study

Case	Number of Mesh Elements	Time Step Size	$\overline{C_V}$(Total)
1	170000	T/300	0.7208
2	210000	T/600	0.7317
3	290000	T/900	0.7280

The validation of the present computational model is carried out by reproducing the results of Lua et al. [10]. As shown in figure 3, the result obtained from the present numerical simulation agrees well with the experiment and the numerical results of Lua et al. [10].

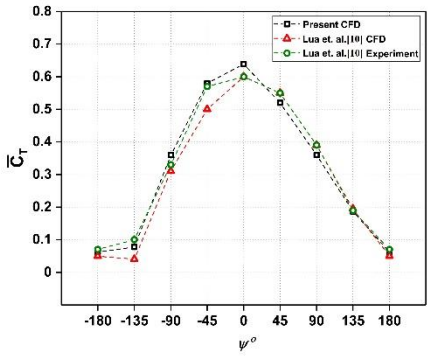

Figure 3: Validation of present computational model.

3 Results and discussion

Cycle-Averaged Force Coefficients

Figure 4(a) shows that the maximum $\overline{C_V}$ is obtained at $\beta = 50^o$ for both the foils, resulting in a peak in total $\overline{C_V}$. The total $\overline{C_V}$ increases with stroke plane angle up to 50°, after that, it decreases. The value of total $\overline{C_V}$ can change heavily by varying the stroke plane angle. The lowest value of total $\overline{C_V}$ (=0.56) is obtained at $\beta = 20^o$ and the highest value of total $\overline{C_V}$ (=1.35) is obtained at $\beta = 50^o$. As shown in figure 4(a), the forefoil $\overline{C_V}$ is greater than hindfoil $\overline{C_V}$ for all cases of β, this shows that the presence of forefoil reduces the performance of hindfoil. Figure 4(b) shows that, the change in forefoil $\overline{C_H}$ is significant as compared to hindfoil by increasing the stroke plane angle. The maximum value of total $\overline{C_H}$ (i.e., maximum drag) is obtained at $\beta = 30^o$ and further increase in the stroke plane angle result in thrust generation. The maximum thrust (negative value represents thrust) is obtained at $\beta = 80^o$. Also, the hindfoil generate thrust for all value of β, whereas the forefoil produces thrust only for $\beta \geq 60^o$.

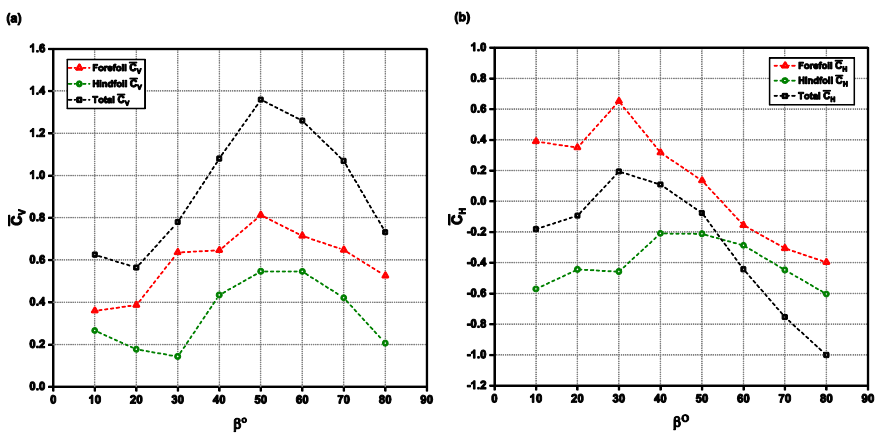

Figure 4: Cycle-averaged vertical ($\overline{C_V}$) and horizontal force ($\overline{C_H}$) coefficient for different stroke plane angle β.

During the upstroke, the hindfoil TEV forms a pair with a CCW vortex generated by the hindfoil trailing edge during the previous downstroke. The strength of the vortex pair and its movement changes for different stroke plane angles. A fluid jet is induced between the vortex pair and is referred to as a dipole jet. The foils experience a reaction force due to the induced dipole jet. The vortex pair generated in each cycle leads to the formation of a vortex street in the wake region. The properties of the dipole jet generated by the vortex pair are studied for different stroke plane angle values.

The properties of the dipole jet are measured at t/T = 0.25 because the maximum value of C_V is obtained near mid-downstroke. The dipole jet for different cases of stroke plane angle is shown with the help of velocity contour in figure 5. The strength of the vortex pair increases with stroke plane angle resulting in a faster dipole jet. In all cases of β, the jet moves downward at a certain angle with the vertical. The inclination angle of the downward jet changes for different stroke plane angles. The reaction force on the foils generated due to the dipole jet can contribute either in thrust or lift depending upon the direction of the dipole jet.

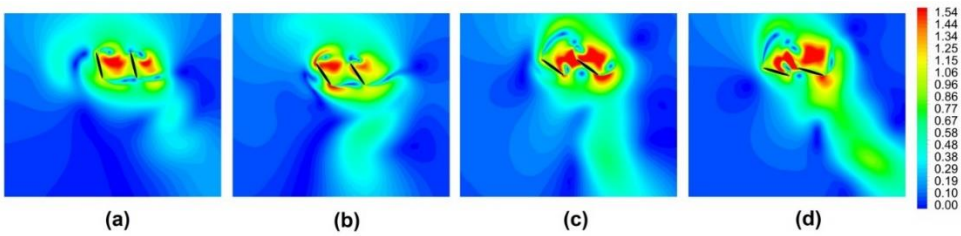

Figure 5: Velocity contours ($u/\ U_R$) during mid-downstroke for four different stroke plane angle cases (a) $\beta = 10^o$ (b) $\beta = 30^o$ (c) $\beta = 50^o$ (d) $\beta = 70^o$

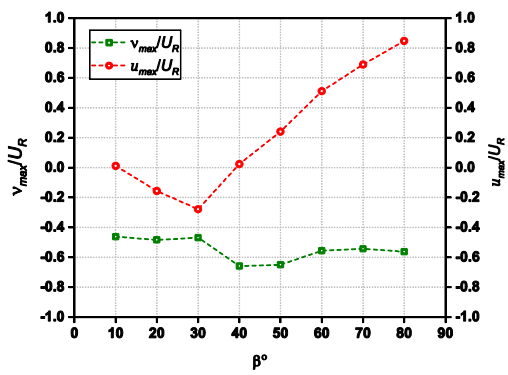

Figure 6: Maximum vertical (v_{max}/U_R) and horizontal (u_{max}/U_R) velocity component of the downward dipole jet during mid-downstroke for different stroke plane angles.

The effect of stroke plane angle on the dipole jet velocity during mid-downstroke is shown in figure 6. The highest value of v_{max}/U_R of the dipole jet is obtained at $\beta = 40^0$. The value of the maximum vertical velocity component increases with β up to $\beta = 40^0$ and then decreases. From figure 6, we can observe that the dipole jet is inclined opposite to the direction of freestream velocity (negative value of u_{max}/U_R) for lower stroke plane angle ($\beta < 40^0$). The highest value of u_{max}/U_R is obtained at $\beta = 80^0$. The value of (u_{max}/U_R) for $\beta = 10^0$ and $\beta = 40^0$ is almost zero, which means the velocity vectors of the dipole jet are nearly vertical for these cases.

The variation of u_{max}/U_R with respect to β, as shown in figure 6 indicates the effect of dipole jet inclination on $\overline{C_H}$. The highest total $\overline{C_H}$ is obtained at $\beta = 30^0$ where the negative peak of u_{max}/U_R is observed. Also, maximum total thrust is obtained at $\beta = 80^0$ where the positive peak of u_{max}/U_R occurs. The value of u_{max}/U_R changes from negative to positive for $30^o < \beta < 80^o$, similarly total $\overline{C_H}$ changes from drag to thrust, as shown in figure 4(b).

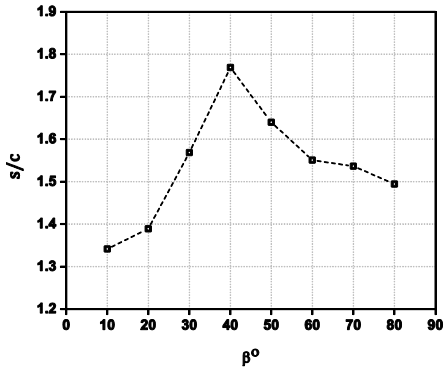

Figure 7: Dipole jet width during mid-downstroke for different stroke plane angles.

The location of vortex pair and dipole jet width (denoted by '*s*'), which is the distance between centroids of counter-rotating vortices, was measured during mid-downstroke from their respective vorticity contour.

The variation in the width of the dipole jet for various stroke plane angles is shown in figure 7. It clearly shows that the dipole jet gets wider with an increase in β up to 40° and gets narrower with a further increase in stroke plane angle. The effect of increasing the inclination of the stroke plane is such that the foils sweep less horizontal distance for a given stroke amplitude (A_o) at higher β and thus results in a narrower jet. Figure 7 shows that the dipole jet is much narrower at $\beta = 50^0$ as compared to $\beta = 40^0$, whereas there is a very small difference in the value of v_{max}/U_R for $\beta = 40^0$ and $\beta = 50^0$ (as shown in figure 6). Hence, the $\overline{C_V}$ obtained for $\beta = 50^0$ is greater than $\beta = 40^0$.

The analysis of the dipole jet with respect to stroke plane angle clearly shows the effect of the wake generated by the foils on the variation of aerodynamic forces. The faster and narrower jet obtained at $\beta = 50^0$ helps the foils to generate the highest $\overline{C_V}$. Also, the highest jet velocity and the inclination of dipole jet along the direction of freestream velocity for $\beta = 80^0$ case results in the maximum value of thrust.

4 Conclusion

The effect of stroke plane angle on the aerodynamic force coefficients during dragonfly take-off flight is studied by performing a two-dimensional numerical simulation of tandem flapping foils oscillating in-phase at $Re = 160$ and $J = 0.1$. The foils are subjected to sinusoidal pitch and plunge motion along an inclined stroke plane and the stroke plane angle is varied from $\beta = 10^o$ to $\beta = 80^o$. It is observed that the hindfoil performance is reduced by the presence of forefoil for low stroke plane angle ($\beta < 40^o$) cases. The maximum vertical force coefficient $\overline{C_V}$ is obtained at $\beta = 50^o$ whereas maximum thrust and drag is obtained at $\beta = 80^o$ and $\beta = 30^o$ respectively. A downward dipole jet is present in the wake region of

the foils for every stroke plane angle. The aerodynamic forces on the foils get affected due to the momentum transfer by the jet. The properties of the dipole jet obtained at each stroke plane angle show the influence of the wake generated by the foils on the variation of aerodynamic forces. These results can help to achieve desired lift during the take-off flight of MAVs.

References

1. Norberg RÅ. Hovering flight of the dragonfly aeschna juncea L., kinematics and aerodynamics. In: *Swimming and flying in nature*. Boston: Springer, 1975, pp:763-781.
2. Choudhry A, Leknys R, Arjomandi M, et al. An insight into the dynamic stall lift characteristics. *Exp Therm Fluid Sci* 2014; 58: 188–208.
3. Dickinson MH, Lehmann FO and Sane SP. Wing rotation and the aerodynamic basis of insect right. *Science* 1999; 284: 1954–1960.
4. Wang ZJ. The role of drag in insect hovering. *J Exp Biol* 2004; 207: 4147–4155.
5. Wang ZJ, Birch JM and Dickinson MH. Unsteady forces and flows in low Reynolds number hovering flight: Two-dimensional computations vs robotic wing experiments. *J Exp Biol* 2004; 207: 449–460.
6. Deepthi S and Vengadesan S. Role of Dipole Jet in Inclined Stroke Plane Kinematics of Insect Flight. *J Bionic Eng* 2020; 17: 161–173.
7. Li Q, Zheng M, Pan T, et al. Experimental and numerical investigation on dragonfly wing and body motion during voluntary take-off. *Sci Rep* 2018; 8: 1011.
8. Shanmugam AR and Sohn CH. Numerical investigation of the aerodynamic performance of dragonfly-like flapping foil in take-off flight. *Proc IMechE Part G: J Aerospace Engineering* 2019; 233: 5801–5815.
9. Gadde SN and Vengadesan S. Lagrangian Coherent Structures in Tandem Flapping Wing Hovering. *J Bionic Eng* 2017; 14: 307–316.
10. Lua KB, Lu H, Zhang XH, et al. Aerodynamics of two-dimensional flapping wings in tandem configuration. *Phys Fluids* 2016; 28: 121901.